2005

Unsteady Tip Leakage, Bow Shock, IGV Wake Interaction in a Compressor

Xuedong Zhou

J. Mitch Wolff
Wright State University - Main Campus, mitch.wolff@wright.edu

 International Journal of Turbo and Jet Engines, 22, 185 - 200 (2005)

Unsteady Tip Leakage, Bow Shock, IGV Wake Interaction in a Compressor

Xuedong Zhou and Mitch Wolff

Department of Mechanical & Materials Engineering, Wright State University, Dayton, Ohio 45435-0001, USA

Abstract

Unsteady aerodynamic analysis of Inlet Guide Vane (IGV)/rotor interaction is conducted with a commercial CFD solver, STAR-CD. 12% and 26% IGV axial chord IGV/Rotor spacing configurations were examined for 100% corrected speed at choke, peak efficiency and near stall conditions to investigate bow shock/tip leakage interaction within blade rows. Comparison with IGV surface unsteady pressure experimental data indicates good agreement at the IGV trailing edge across the span for both spacing configurations; therefore, validating the modeling of the high speed, highly loaded transonic compressor. The strongest effect on the tip clearance flow physics was caused by decreasing the axial spacing. The 12% axial spacing, baseline configuration had a significant effect on the cross location of the leading edge tip vortex and the rotor bow shock (i.e. the lambda shaped interaction region). In addition, the double leakage moved downstream of the bow shock due to the IGV wake for the close spacing. At 26% axial spacing, the IGV wake influence was not significant. The back pressure influence was important. The high loading at the near stall condition prevented any significant IGV wake interaction effect on the tip clearance flow. For the chocked flow condition, the bow shock structure change (going from a normal shock to an oblique shock) reduces the bow shock strength. The IGV wake caused the tip vortex to intensify, this is mainly caused by a decrease in the bow shock strength. Vortex breakdown occurs due to deceleration after passing a strong shock, which for the choked case does not happen until the vortex reaches the passage shock.

Keywords: Transonic Compressor, Tip Leakage, Wake/Bow Shock Interaction

1.0 Introduction

With the development of modern jet engines, thrust-to-weight ratio has been greatly improved over the past half century by in part reducing the overall length of the compressor; therefore the aerodynamic unsteadiness inside turbomachinery has been significantly increased. To improve the reliability and efficiency, phenomenon, like, high cycle fatigue (HCF) and tip clearance flows, have been investigated by many researchers. With the increased power of computers and computer simulation software, computation fluid dynamics (CFD) is widely used for jet engine design due to its relatively low cost and short design cycle. However, there are still many issues that need addressed in utilizing CFD to model modern jet engines, in particular the unsteady flow effects of IGV/rotor interaction on tip clearance flows in a transonic compressor.

Tip clearance flow remains a topic attracting many researchers due to its importance for compressor performance and stability. The structure and physics of tip clearance flows have been investigated by many researchers. The Lambda shaped interaction between the tip vortex and passage shock near the end wall increase rotor blockage /1,2/, which reduces stage efficiency, flow range and pressure rise /3/. Also, tip clearance flow plays an important role on compressor stall /4/. However, the intensity of the tip vortex does not necessarily increase blockage. Recently, Furukawa *et al.* /5,6/ pointed out that the breakdown of the tip leakage vortex is the direct cause of the low-energy flow region. The breakdown of the vortex substantially changed the behavior of the end wall

boundary layer and passage blockage so that it could significantly degrade compressor performance.

The upstream stator wakes also influence the tip flow by functioning as a negative jet. The jet produces a pressure disturbance and could generate a local stagnation point on the downstream rotor suction surface /7,8,9/. Double leakage can be avoided by deflecting the tip clearance flow with this local stagnation point.

However, few studies have investigated upstream wake influence on the rotor bow shock/tip leakage vortex interaction in a transonic compressor. In addition, most studies focus on either steady state or time average parameters for analysis. Therefore, the unsteady characteristics of the interaction phenomena in a transonic compressor have not been thoroughly investigated. To obtain more insight into the unsteady flow physics details, this paper concentrates on the unsteady aerodynamics in a transonic axial compressor configuration to address the following issues:

1. Unsteady wake influence on tip vortex/blade row shock interaction.
2. Unsteady wake influence on double leakage.
3. Axial spacing influence on unsteady wake, and shock/tip leakage vortex interaction.
4. Back pressure influence on unsteady wake, and shock/tip leakage vortex interaction.

2.0 Experimental Facility

The Compressor Aero Research Lab (CARL) Stage Matching Investigation (SMI) facility at Wright-Patterson Air Force Base is a high-speed, highly loaded compression stage. The transonic rig comprises an inlet guide vane (IGV), single-stage core compressor consisting of a rotor and stator with 24, 33 and 49 airfoils, respectively, each with a 19-in. tip diameter. Axial spacing between IGV and rotor can be adjusted to 12%, 26% and 56% of IGV chord (referred to as close, mid and far spacing). IGV surface unsteady pressure experimental results have been reported by Hutton *et al.*/10/ using a high spatial resolution, high frequency response flexible pressure sensor array. Only 100% speed conditions will be analyzed for three back pressure settings (near stall, peak efficiency, and choked).

3.0 CFD Simulation Model

3.1 CFD Solver and Turbulence Model

A commercial finite volume method solver, STAR-CD, is employed to solve the 3-D Navier-Stokes equations for the CARL/SMI rig. Since the experimental data shows very few separation regions throughout the flow domain, the near wall region is computed by wall functions with Chen's $k-\varepsilon$ turbulence model utilized for all CFD predictions presented.

3.2 Computational Grid

The SMI facility has 24 IGV and 33 rotor blades. The ideal model would include 8 IGV and 11 rotor blades, which will be expensive computationally due to the lack of phase lagged boundary conditions in STAR-CD. Therefore, 33 IGV blades is assumed for the computational model.

Capped-O meshes are used with a 5-chord stretched H-grid extension at both the inlet and exit plane to reduce wave reflections because non-reflecting boundary conditions are not available. Several different mesh sizes have been tested as a grid independence study. The Capped-O mesh is the most critical grid for the blade flow physics. Therefore, only the mesh surrounding the blades will be described. For the IGV O-grid, there are 241 grid points around the blade, 41 points from the blade to the periodic boundary and 57 points spanwise i.e. 241x41x57. The corresponding rotor O-grid is 161x33x57. Fig. 1 shows the basic topology of the Capped O-mesh used in the following close spacing simulation. Some grid points have been omitted for clarity.

The grid in the tip clearance region is shown in Figs. 2 and 3. It has 161 points in the O-direction, 9 points from the chamber line to the blade surface, Fig 2, and 7 points spanwise for the tip clearance height, Fig. 3. The tip clearance of the test facility is

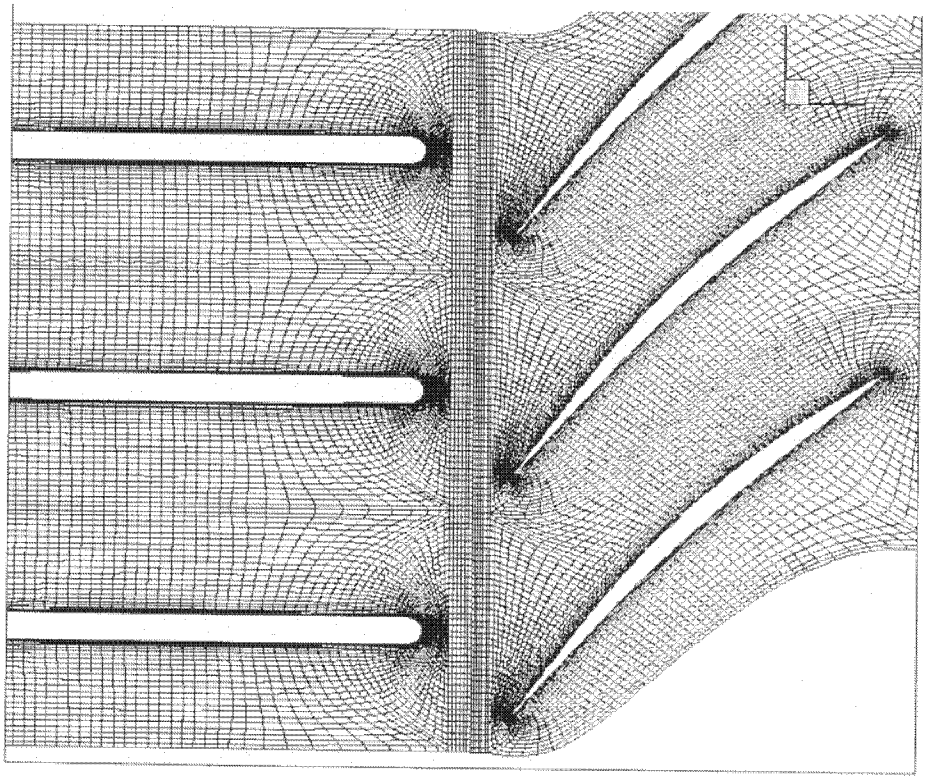

Fig. 1: Capped-O Meshes

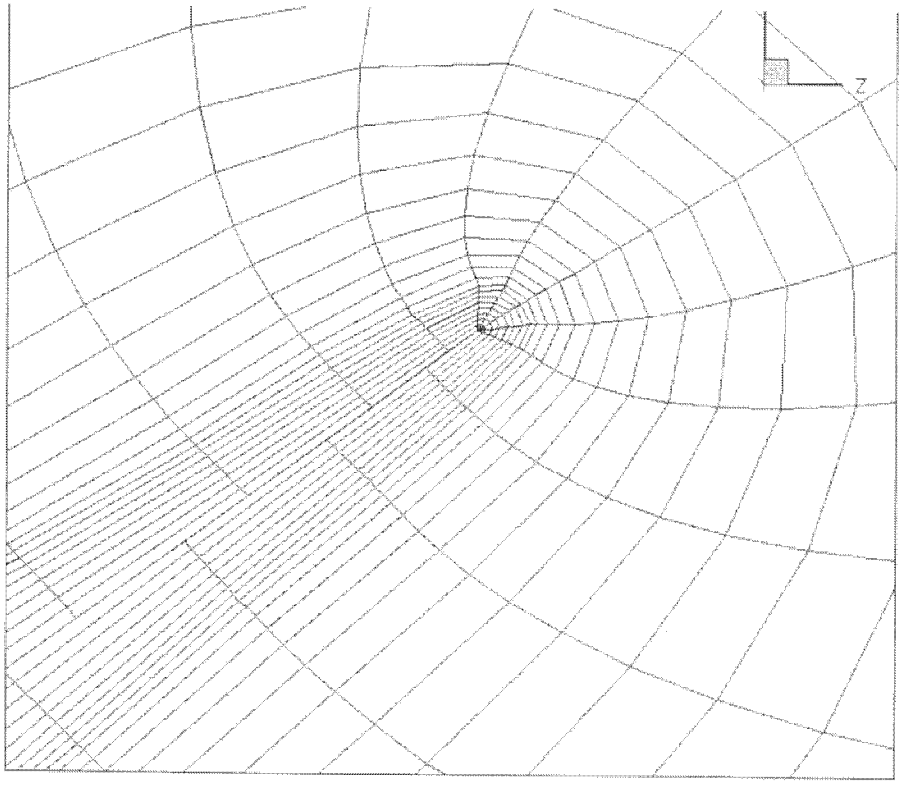

Fig. 2: Tip Clearance: Top View at Trailing Edge

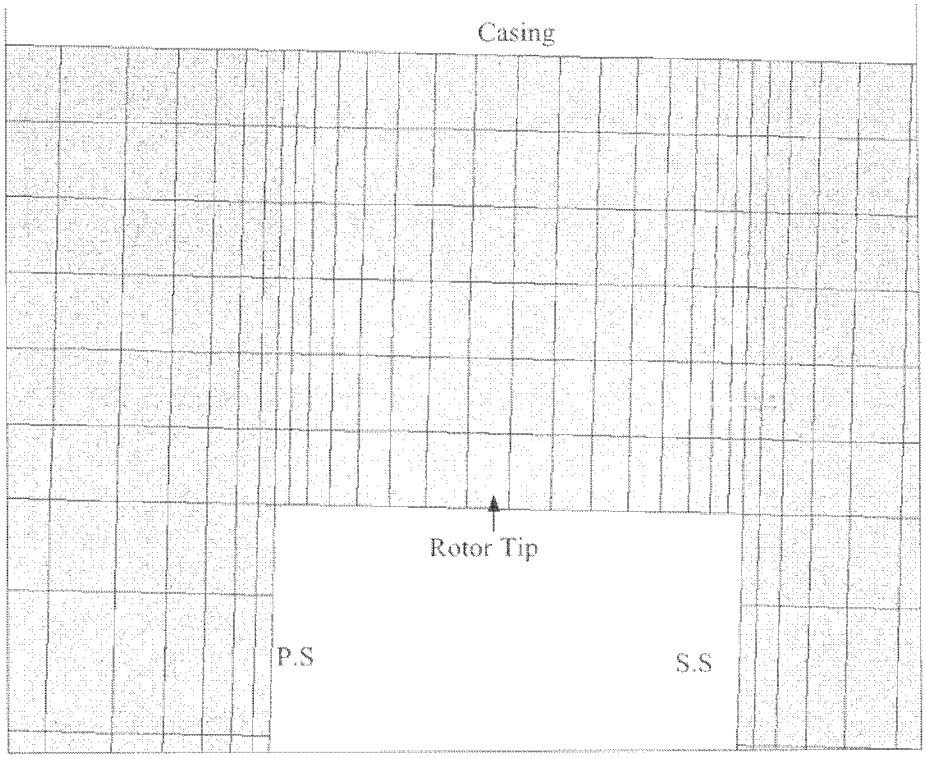

Fig. 3: Tip Clearance: Axial View

0.015 inch.

Grid points are clustering towards the blade surface and end walls to ensure y+ values at the first cell are in the 30~100 range over the whole flow field for the high Reynolds number wall boundary simulation using wall functions.

3.3 Boundary Conditions

Stagnation pressure and temperature is assigned at the inlet plane while the exit plane boundary condition imposes a fixed pressure profile. Wall boundary conditions are applied to both blades and end walls, while the rest of the boundaries use periodic boundary conditions.

3.4 Computational Details

The gap between the IGV and rotor blade has 41 grid points evenly distributed circumferentially. Unsteady simulations with a moving rotor mesh have a fixed time step of 1.122×10^{-6} s to ensure 3 steps per cell and 120 steps per passage. The mean CFL number is approximately 0.5 throughout the simulation.

Each unsteady analysis starts from a nearly converged steady state solution and takes about one revolution to achieve a converged unsteady prediction. When converged, the mass flow rate is within 0.2% of the experimental data and the pressure history shows a repeatable oscillation cycle based on the blade pass frequency.

3.5 Computational Convergence Criteria

Due to the nature of the unsteady flow, the back pressure has to be adjusted slightly to be within 0.2% of the experimental mass flow rate data to ensure the same operating points. Convergence is reached only after both inlet and outlet mass flow rates become periodic and the mean values maintain a nearly constant level for one whole revolution.

4.0 Results and Discussion

The 12% and 26% IGV chord axial spacing between the IGV and rotor blade rows for the peak efficiency back pressure is simulated and results are compared against experimental data acquired and analyzed previously /10/ to determine the accuracy of the CFD code and models utilized. Only the IGV and rotor blade rows have been modeled in the CFD analysis. The experimental data has been obtained with the stators included. Since the interaction being investigated is primarily driven by the IGV/rotor effects, the influence of the stators on the analysis is not significant and can be ignored. Once the validity of the computational models have been confirmed, then a detailed investigation into the unsteady interaction of the IGV wake, tip clearance leakage vortex and rotor bow shock will be presented. Two different time snapshots of the interaction will be selected. The first snapshot will be before the IGV wake reaches the rotor bow shock and will be referred to as "instance 1". The second snapshot will be after the IGV wake has passed through the bow shock and will be referred to as "instance 2". Then the significant effects of variations in IGV/rotor axial spacing and back pressure on the tip clearance flow physics at these two slices in time will be investigated to highlight the importance of the unsteady flow interactions.

4.1 IGV/Rotor Blade Row Interaction

Since the CFD model has been simplified to utilize a one-to-one IGV to rotor blade ratio, the phase difference between the two instrumented IGV surfaces will be altered. So, analyzing the pressure difference across the IGV is not the appropriate method to compare the computational and experimental results. It is more appropriate to make a direct comparison to the unsteady experimental data on each surface of the IGV. Therefore, a comparison is made between the unsteady pressure response history on the two IGV blade surfaces (#1 and #2) separately. For ease of interpeting the results, each blade passage is repeated so that two blade passages are shown.

4.1.1 26% IGV Chord Axial Spacing Configuration

Figs. 4 and 5 show the Cp time history at 95% and 90% IGV chord location for two span locations, 80% and 95%, respectively. At 95% chord, the computational analysis predicts an unsteady pressure oscillation magnitude with slight errors compared to the experimental data. The phase difference for IGV surface 2 is due to the modified blade count effect. However, at 90% chord location the computational solution shows a stronger decay than the experimental data or a reduced unsteady amplitude. As Gorell *et al.* /11/ mentioned the oblique shock detached from the LE of downstream rotor is separated by the IGV TE and becomes a partially normal shock traveling upstream. A closer pitch dimension with 33 IGV blades instead of 24 blades, results in bow shocks at the IGV upper and lower surface having a stronger interaction which raises the overall pressure level in the passage. But the unsteady pressure fluctuations generated are decreased due to shorted pitch dimension.

Comparisons at lower spanwise locations also show excellent agreement with the experimental data. They are not presented because they are not closely related to the tip clearance flow being investigated in this study.

4.1.2. 12% IGV Chord Axial Spacing Configuration

Figs. 6 and 7 show the pressure coefficient history for the 12% IGV chord axial spacing configuration at 95% and 90% chord location for two spanwise locations 80% and 95%, respectively. Due to the smaller gap between blade rows, the bow shock interaction is even stronger resulting in an increase in the IGV surface unsteady pressures. At 95% chord, the predicted surface unsteady pressure oscillation magnitude agrees very well with the experimental data. However, unlike the 26% spacing results, at the 90% chordwise location, the computational results indicate only a slight unsteady magnitude decay greater than the experimental data. Since both the mesh and temporal algorithm utilized are basically identical to the 26% configuration, it is

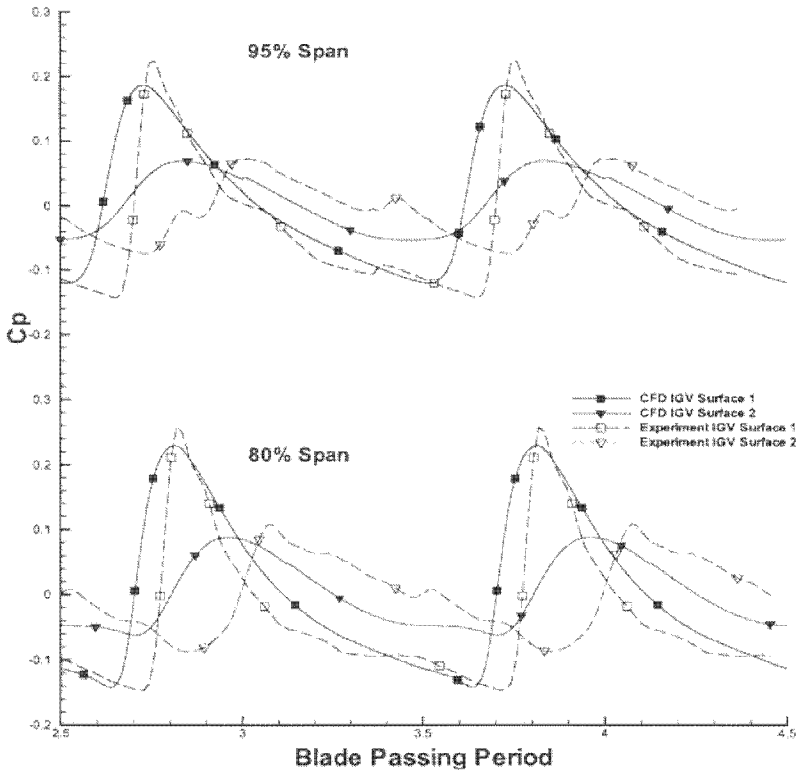

Fig. 4: Pressure coefficient at 95% chord location for the 26% axial spacing configuration

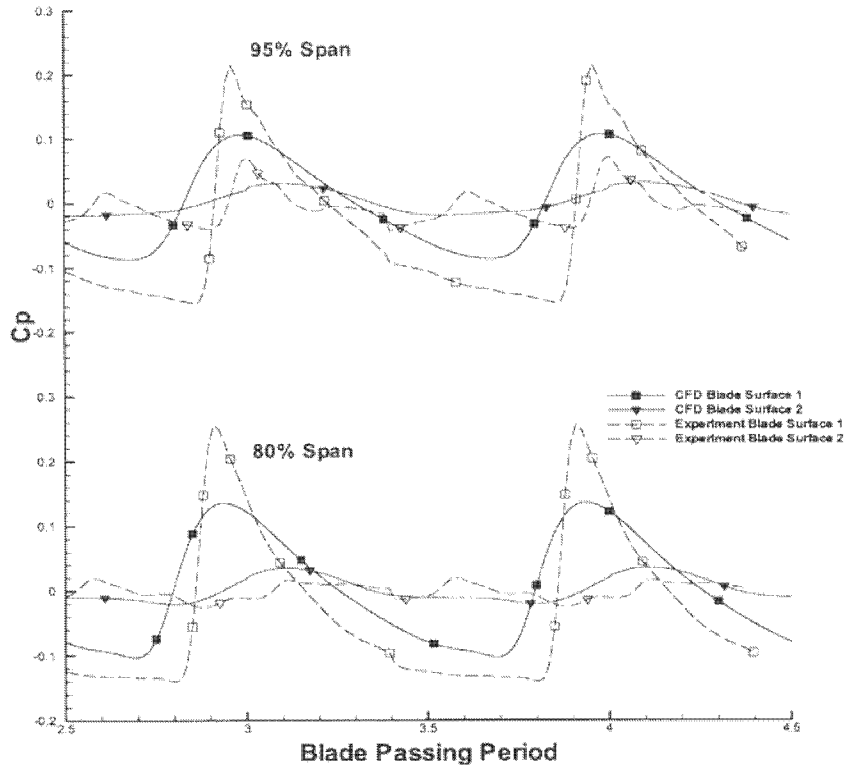

Fig. 5: Pressure coefficient at 90% chord location for the 26% axial spacing configuration

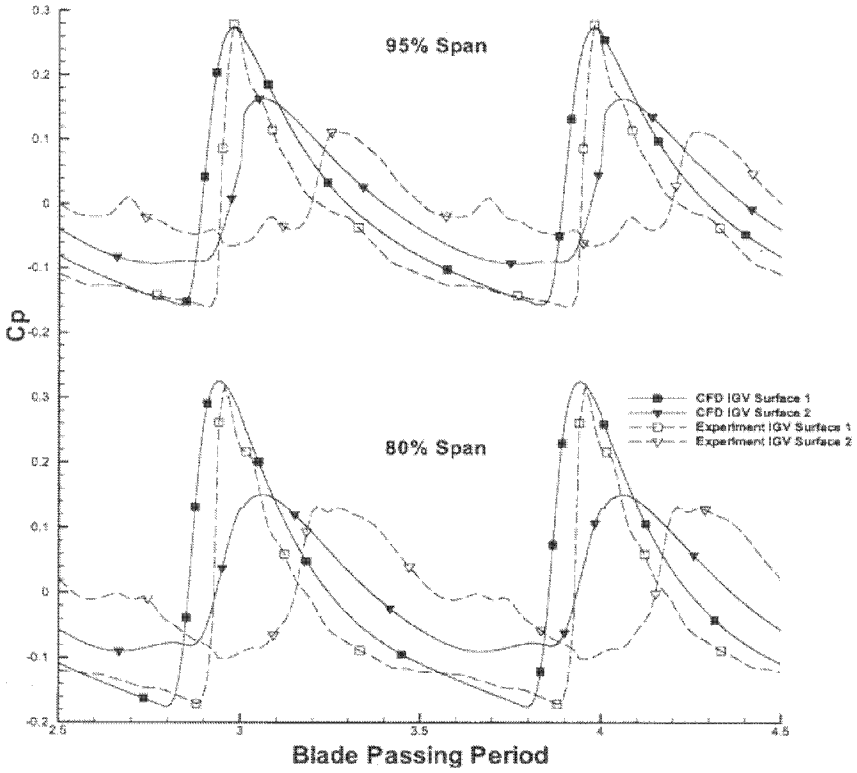

Fig. 6: Pressure coefficient at 95% chord location for the 12% axial spacing configuration

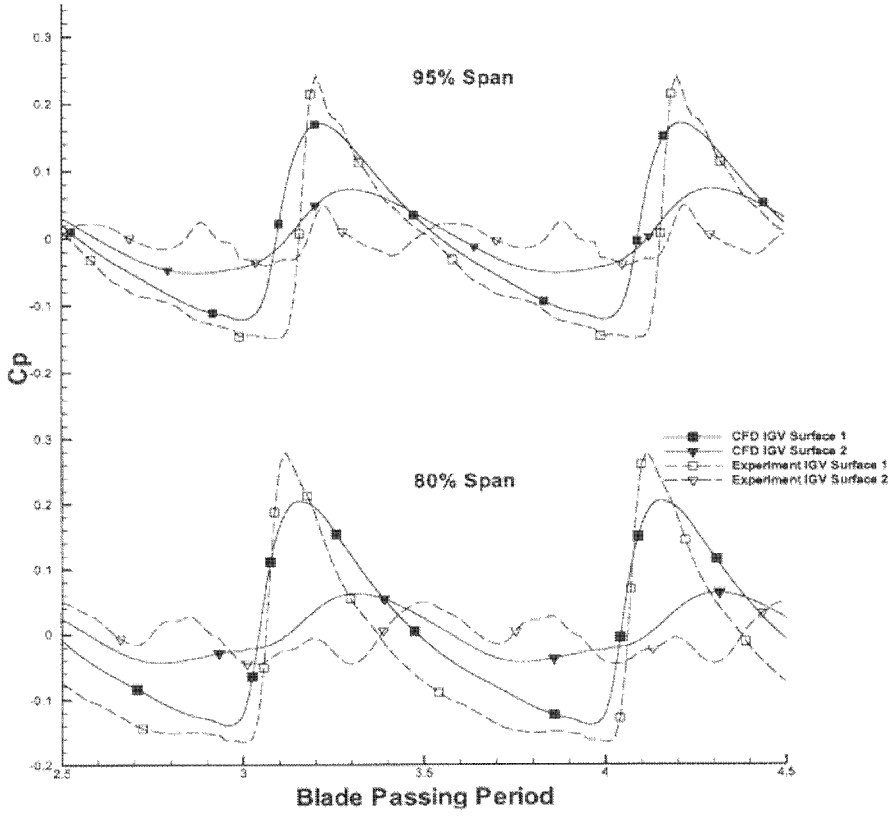

Fig. 7: Pressure coefficient at 90% chord location for the 12% axial spacing configuration

reasonable to conclude that the slower magnitude decay is due mainly to the decreased axial spacing between the two blade rows.

Overall, the computational simulations for both the mid and close IGV/rotor axial spacing configurations yield very reasonable agreement with the IGV surface unsteady pressure experimental data at several spanwise and chordwise locations. The excellent agreement at 95% span is a good indication of accurate modeling of both the IGV wake and rotor tip clearance flow. Therefore, detailed investigations of the unsteady flow interactions with the tip clearance flow for this transonic compressor configuration are appropriate and will be presented.

4.2 Tip Leakage Vortex, Upstream Wake and Bow Shock Interaction

Furukawa *et al.* /5,6/ studied the vortex breakdown and its influence on compressor performance based on time average predictions. In the current paper, more insight will be given on wake influence of bow shock/tip vortex interaction by investigating time instants of the unsteady flow analysis when the IGV wake is in two different locations relative to the rotor bow shock as previously discussed. A detailed investigation will be made of the unsteady IGV/rotor interaction effects on the tip leakage vortex flow field. In particular, the influence of variations in the IGV/rotor axial spacing and stage back pressure on the IGV wake/bow shock/tip vortex unsteady interaction will be presented.

For a better understanding and review of tip vortex behavior, it is necessary to introduce a term called normalized helicity, proposed initially by Furukawa *et al.* /5/

$$Hn = \frac{\vec{\xi} \cdot \vec{w}}{\left|\vec{\xi}\right| \left|\vec{w}\right|} \qquad (1)$$

where $\vec{\xi}$ and $\vec{w}$ are the absolute vorticity and relative velocity vectors, respectively. Absolute vorticity is used because the secondary flows in the rotor are dominated by the absolute vorticity along the relative velocity direction /5/. Therefore, normalized helicity denotes the cosine of the angle between the vorticity and relative velocity. *Hn* becomes unity at the vortex core and changes sign to indicate a vortex reverseral. When its value goes from unity to zero, it means that the vortex structure has broken down (i.e. vortex breakdown). To capture the details of a vortex core breakdown requires a high-resolution grid; however, by utilizing the normalized helicity tip leakage vortex breakdown can be captured and investigated with a coarser mesh. Therefore, a detailed investigation into the effect of blade row axial spacing and back pressure variation on the IGV wake, bow shock and tip leakage vortex interaction unsteady flow physics will be presented.

4.2.1 Baseline Model: 12% Axial Spacing at Peak Efficiency

At 12% axial spacing, two time instants are studied for the IGV wake effect with the rotor bow shock in the tip region. Fig. 8 (a-b) shows when the wake is behind the blade row bow shock, while Fig. 9 illustrates when the wake is in front of the rotor bow shock. Blade row contour lines (Fig. 8b) indicate the static pressure field near the casing wall. Color contour slices (Fig. 8a) represent the relative velocity magnitude. Finally, the streamline traces (Fig. 8(a-b)) are colored with the normalized helicity, *Hn* value, with white representing 1, black = -1 and grey = 0.

As shown in Fig. 8(b), the wake is at 40% pitch from the suction surface and behind the bow shock. So, the IGV wake directly points at the suction surface of rotor blade. Therefore, the high pressure disturbance in the negative wake jet also passes through part of the tip vortex. Consequently, the pressure troughs nearby are slightly "pushed" downstream. However, the bow shock is distorted only slightly. Therefore, the cross location of the neighboring bow shock and tip leakage vortex traveling downstream towards the rotor suction surface is slightly affected. This negative jet also produces a relative location stagnation spot on the rotor blade suction surface, which further diverts the tip clearance flow through this region. Fig. 8(b)

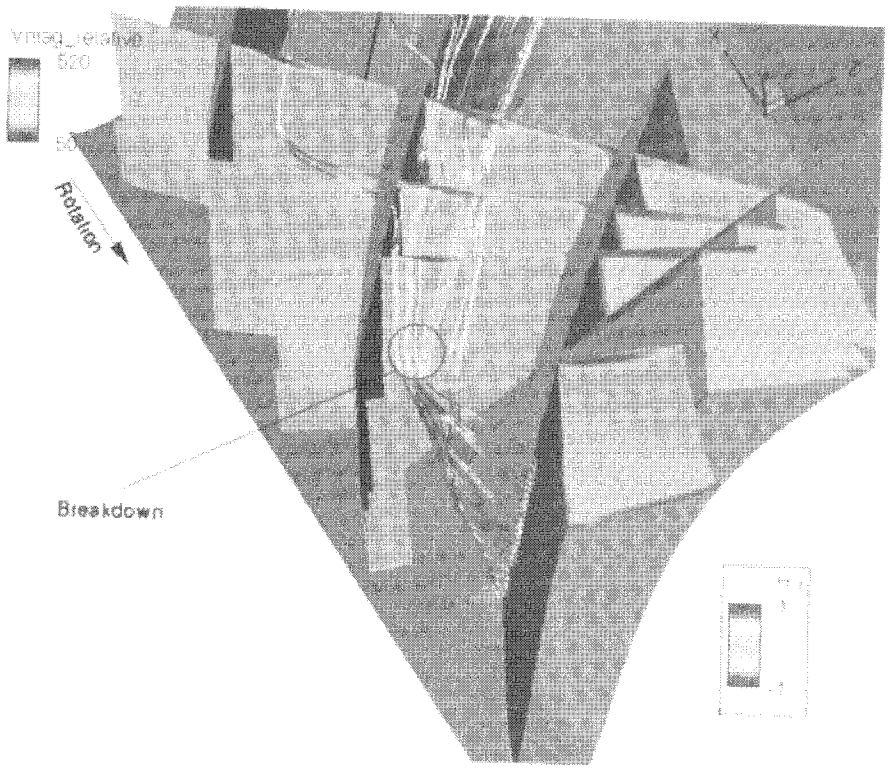

Fig. 8(a): 1st time instant at 12% spacing, peak efficiency

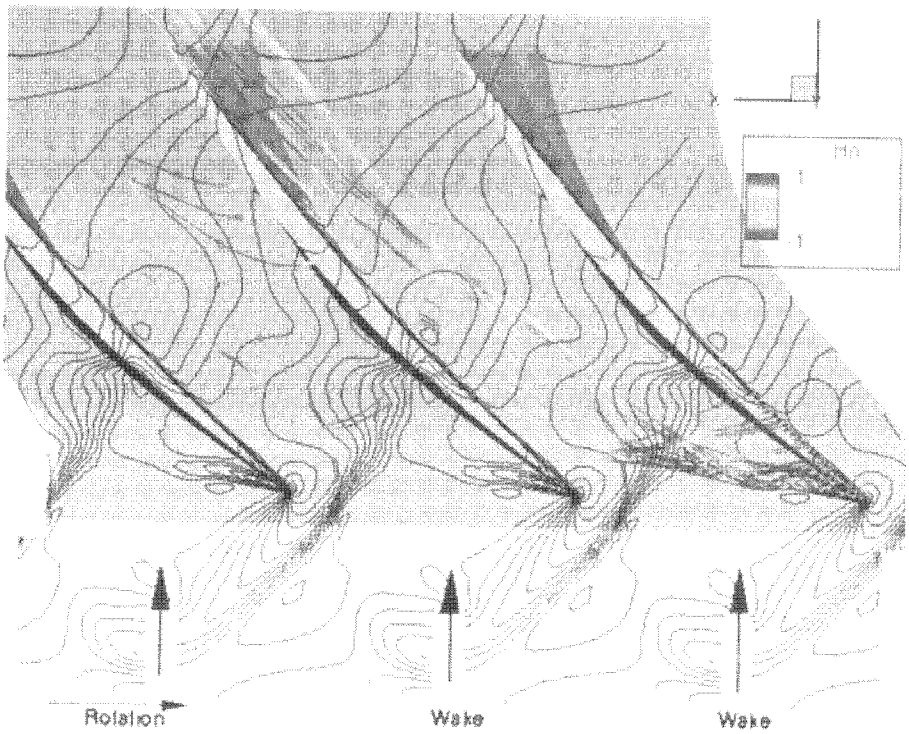

Fig. 8(b): 1st time instant at 12% spacing, peak efficiency

shows a few streamlines going through a neighboring blade tip gap. This forms a phenomenon called 'double leakage'. However, due to the above-mentioned location stagnation point, the location at which double leakage occurs is moved further downstream after the bow shock at this time instance.

In Fig. 9 – time instance 2 – the IGV wake is closer to the pressure side and in front of the rotor bow shock. The bow shock is bent due to the wake disturbance. The wake disturbance is weakened by the bow shock. Due to the wake position, its influence on the tip clearance vortex is marginal. Compared with Fig. 8(b), the pressure troughs at the rotor leading edge tip are largely intact and identical to results at time instance 1. Therefore, the cross location of the leading edge tip vortex and bow shock is brought towards the mid-pitch region and upstream slightly. This is detrimental to the compressor performance since it will bust the tip vortex earlier in the flow. As discussed by Adamczyk *et al.* /1/, this lambda shaped interaction will cause highly rotational flow and large separation near stall. Finally, the double leakage at this time instant moves upstream in front of the bow shock.

In both Figs. 8 and 9, the stream trace contours are colored with the normalized helicity, white denoting a normalized helicity of 1 and grey a value of 0. As mentioned earlier, the transition of helicity from unity to zero indicates when tip leakage vortex breakdown occurs.

Both Figs. 8 and 9 show the normalized helicity transitioning to zero shortly after the streamline trace passes through the bow shock. The relative velocity magnitude at different cuts normal to the stream trace indicates an area of low relative velocity. This area expands drastically after the vortex breakdown occurs. This is an indication of a low-energy flow zone that acts as an obstacle in the passage. Its existence substantially increases casing boundary thickness and passage blockage.

4.2.2 Spacing Influence: 26% Spacing at Peak Efficiency

Figs. 10 and 11 depict the same time instants as

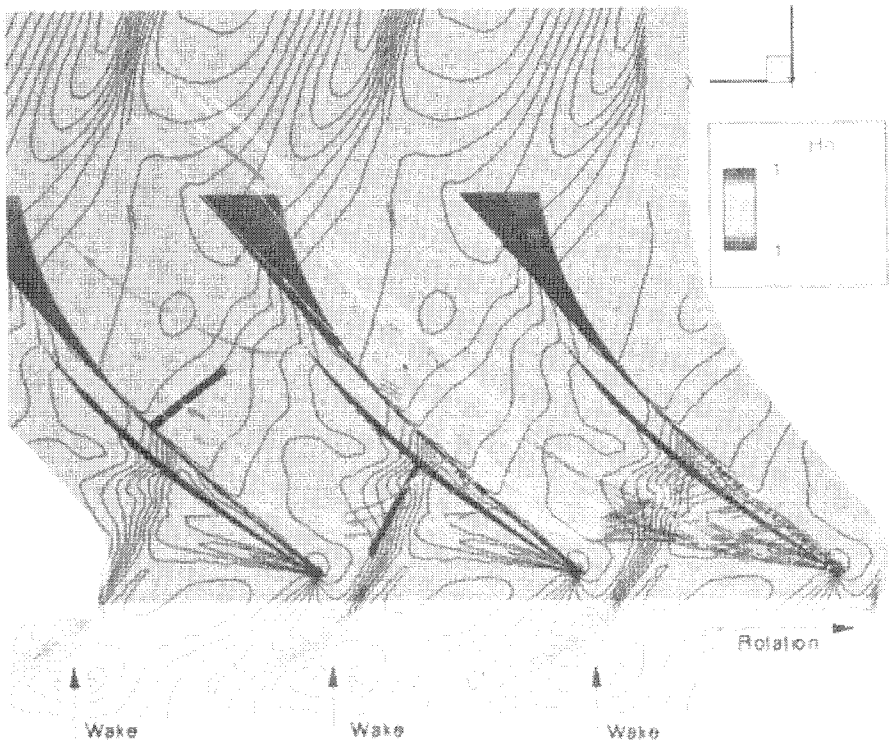

Fig. 9: 2nd time instant at 12% spacing, peak efficiency

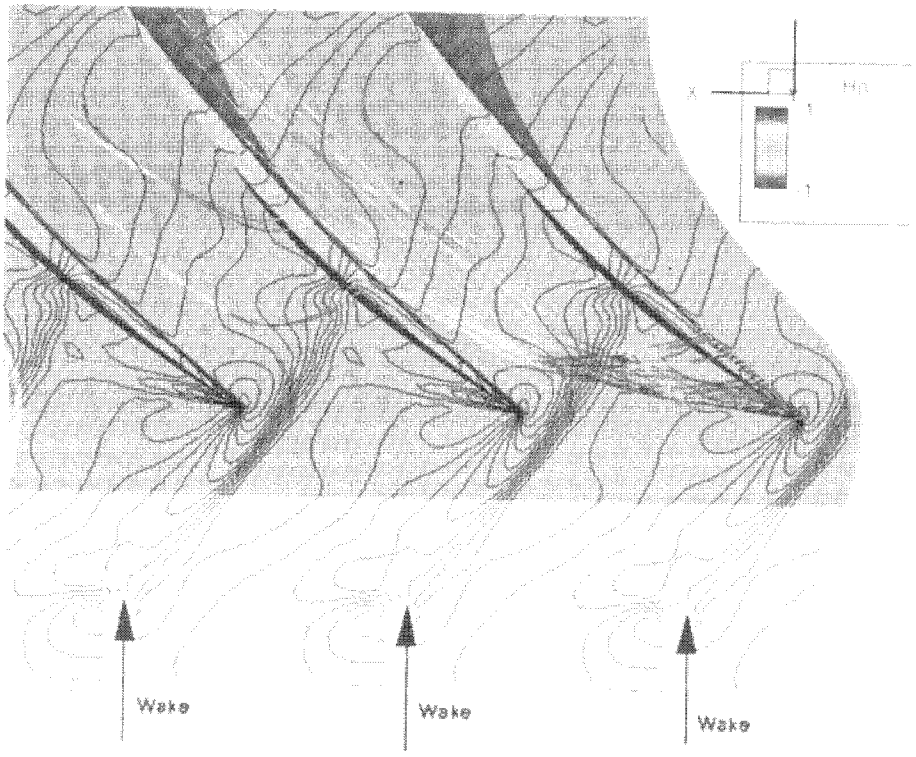

Fig. 10: 1st time instant at 26% spacing, peak efficiency

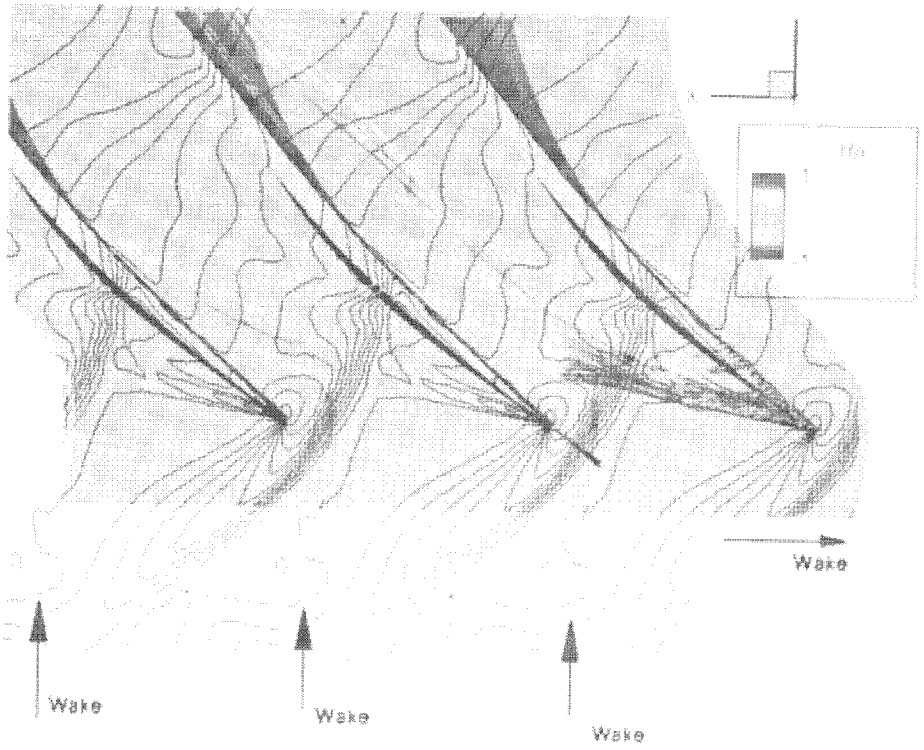

Fig. 11: 2nd time instant at 26% spacing, peak efficiency

Figs. 8 and 9 only for the 26% IGV chord axial spacing configuration. Due to the increased spacing between the blade rows, the tip vortex is not exposed directly to wake. Therefore, the IGV wake influence on the leakage flow is reduced. Near the casing wall, the pressure contours at the rotor leading edge indicate that the leakage flow is almost identical for the two different time snapshots. Therefore, at 26% spacing IGV wake influence on the leading edge tip leakage vortex is trivial. In both Figs. 10 and 11, the streamlines pass through the neighboring blade tip gap which indicates a double leakage for this spacing configuration. However, due to the increased gap IGV wake influence on the double leakage region is minor. In contrast to the 12% spacing configuration, the 26% spacing configuration shows only minor differences in the double leakage location caused by the IGV wake.

At the second time instant Fig. 11, the bow shock is once again bent due to the wake disturbance, but the change of angle is smaller than the 12% spacing case. Like in the close configuration analysis, the normalized helicity indicates that the tip vortex is strongly affected by the bow shock such that vortex breakdown occurs after the shock.

4.2.3 Back Pressure Effects: Near Stall 12% Axial Spacing

The near stall operating condition has the highest pressure ratio and the lowest mass flow rate. At this operating point, the rotor bow shock stands the furthest upstream of the rotor leading edge. Fig. 13, containing the second time instant, shows that the bow shock is basically unaffected by the wake (i.e. straight shock front). This indicates the shock strength is higher than the baseline model due to its high loading. In addition, Fig. 12 shows the leading edge tip leakage flow generated by this highly loaded rotor is barely affected by the wake. With the high loading at near stall, the high pressure in the neighboring blade pressure surface prevents streamlines originating from the leading edge tip clearance from passing through the adjacent tip clearance. Only flow originating from the 40% chord location produces double leakage. Therefore,

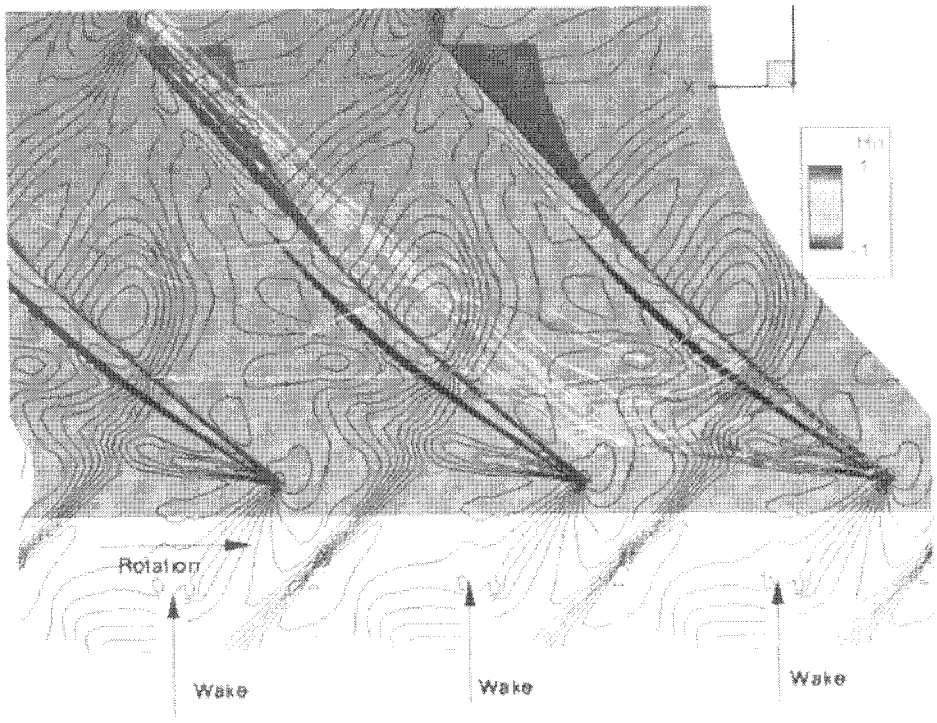

Fig. 12: 12% spacing 1st time instant near stall back pressure

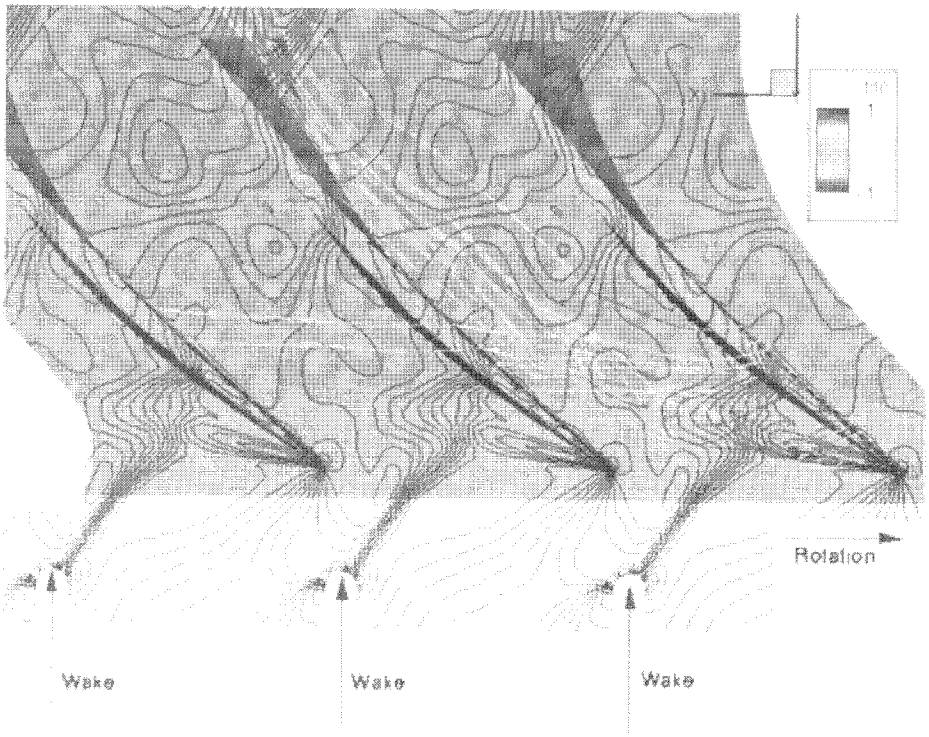

Fig. 13: 12% spacing 2nd time instant near stall back pressure

the higher blade loading reduces the double leakage. Finally, the tip vortex breakdown location stays consistent relative to the bow shock position or the vortex breakdown occurs right after passing through the bow shock.

4.2.4 Back Pressure Effects: Choked 12% Axial Spacing

For the choked flow back pressure, the bow shock is an oblique shock attached to the rotor leading edge. In addition, there is a passage shock on the suction surface at about 40% chord from leading edge. As shown in Fig. 14, the pressure trough near the leading edge of the suction surface changed its direction after passing though the IGV wake disturbance. Compared with Fig. 15, Fig.14 also shows that the oblique shock is chopped by the tip clearance flow. Therefore, the tip vortex has been intensified by the IGV wake. The tip vortex breakdown for the choked back pressure configuration occurs when the tip vortex passes through the downstream passage shock, not the rotor bow shock as in all the previous results presented. Finally, Fig. 16 shows the boundary thickness on the suction surface undergoing considerable expansion due to the relative velocity decelerate after the passage shock which is consistant with an off design analysis.

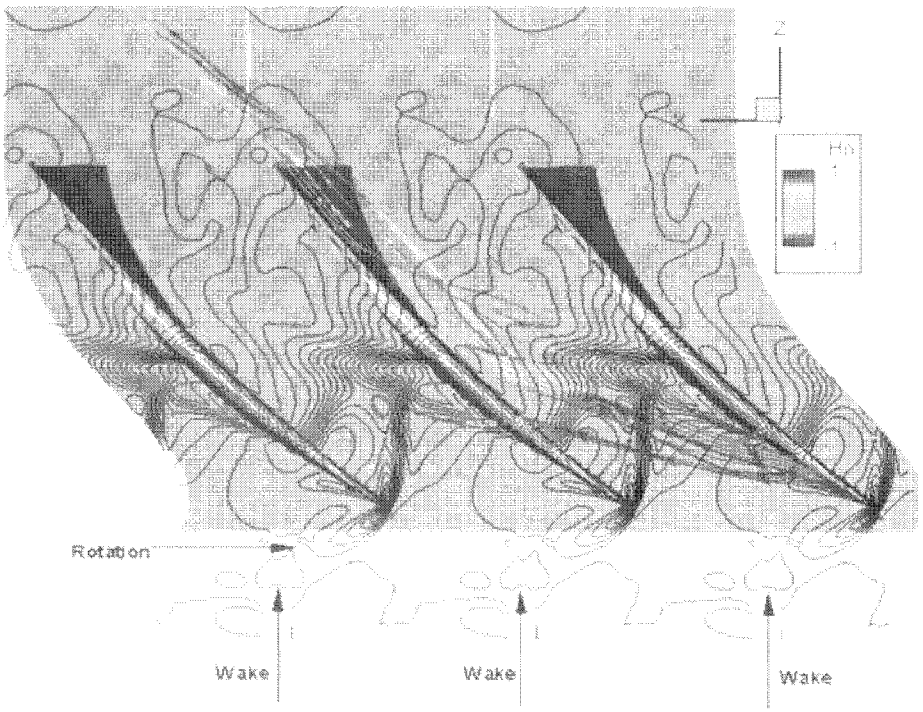

Fig. 14: 12% spacing 1st time instant choked back pressure

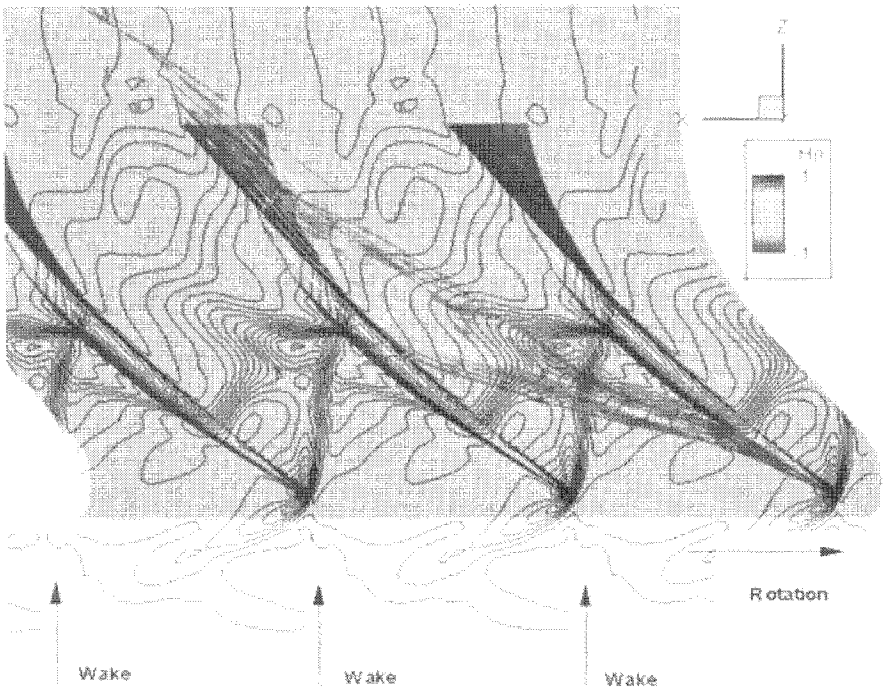

Fig. 15: 12% spacing 2nd time instant choked back pressure

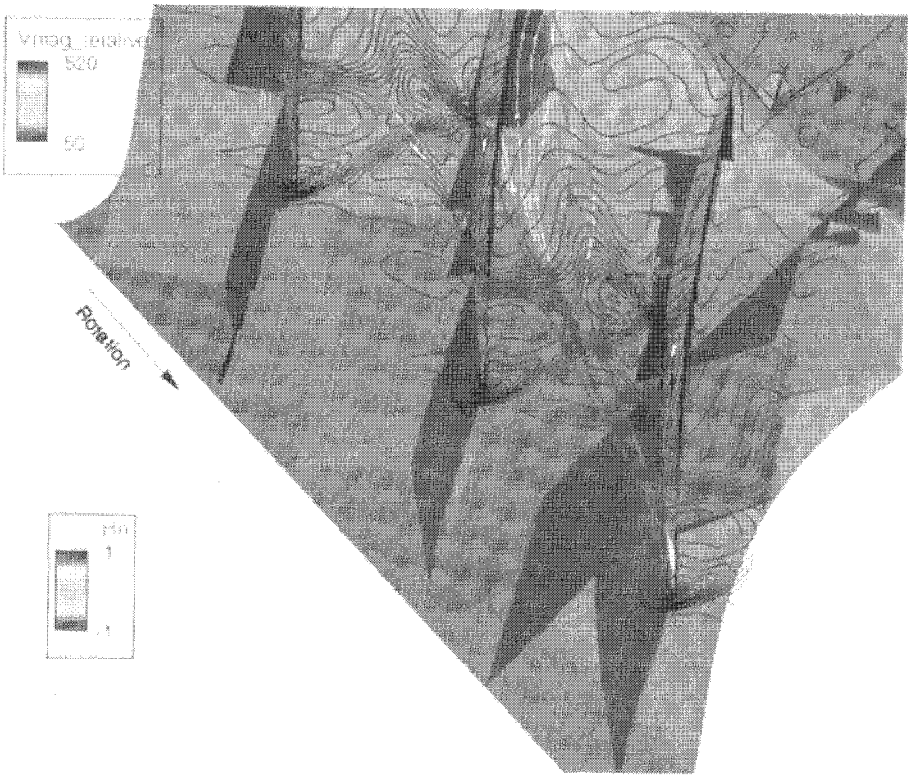

Fig. 16: 12% spacing 2nd time instant choked back pressure

5.0 Summary and Conclusion

A computational investigation of the tip clearance unsteady aerodynamics associated with variations in the axial spacing and back pressure for a highly loaded, high speed, transonic compressor has been accomplished. The commerical CFD solver, Star-CD, was initially validated for the CARL/SMI facility by comparison of IGV surface unsteady pressures with previously obtained experimental data. An execellent agreement was shown, thereby validating the method. The tip flow unsteady aerodynamics was then investigated. The strongest wake effect on the tip clearance flow physics was caused by changing the axial spacing. The 12% axial spacing, baseline configuration had a significant effect on the cross location of the leading edge tip vortex and the rotor bow shock (i.e. the lambda shaped interaction region). This is detrimental to the compressor performance. In addition, the double leakage moved downstream of the bow shock for the close spacing due to wake disturbance. At 26% axial spacing, the IGV wake influence was not significant. The back pressure influence was important. The high loading at the near stall condition prevented any significant IGV wake interaction effect on the tip clearance flow. For the chocked flow condition, the bow shock structure change (going from a normal shock to an oblique shock) reduces the bow shock strength. The IGV wake caused the tip vortex to intensify, this is mainly caused by a decrease to the bow shock strength. Vortex breakdown occurs due to deceleration after passing a strong shock, which for the choked flow case does not happen until the vortex reaches the passage shock.

6.0 Acknowledgement

The authors want to acknowledge Tim Leger, Tim Hutton and Dr. David Johnston for their help

with the experimental data and computational tools. In addition, the support of ADAPCO, Inc. developers of the STAR-CD CFD model is greatly appreciated. Finally, the financial support of the Dayton Area Graduate Studies Institute (DAGSI) and the College of Engineering and Computer Science is most gratefully acknowledged.

References:

1. Adamczyk, J., Celestina, M. L., and Greitzer, E. M., "The role of tip clearance in high speed fan stall," *ASME Journal of Turbomachinery*, Vol. 115, pp. 28-39, Jan. 1993.
2. Khalid, S. A., Khalsa, A. S., and Waitz, I. A., "Endwall blockage in axial compressors," *ASME Journal of Turbomachinery*, Vol. 121, pp. 499-509, July, 1999.
3. Suder, K., "Blockage development in a transonic, axial compressor rotor," *ASME Journal of Turbomachinery*, Vol. 120, pp. 465-476, July, 1998.
4. Hoeger, M., Fritsch, G., and Bauer D. "Numerical simulation of the shock-tip leakage vortex interaction in a HPC front stage," *ASME Journal of Turbomachinery*, Vol. 121, pp. 456-468, July, 1999.
5. Furukawa, M., Saiki, K., Nagayoshi, K., Kuroumaru, M., and Inoue, M., "Effects of stream surface inclination of tip leakage flow fields in compressor rotors," *ASME Journal of Turbomachinery*, Vol. 120, pp. 683-692, Oct. 1998.
6. Furukawa, M., Inoue, M., Saiki, K., and Yamada, K., "The role of tip leakage vortex breakdown in compressor rotor aerodynamics," *ASME Journal of Turbomachinery*, Vol. 121, pp. 469-480, July 1999.
7. Sirakov, B. T., and Tan, C. S., "Effect of unsteady stator wake –rotor double leakage tip clearance flow interaction on time-average compressor proformance," *ASME Journal of Turbomachinery*, Vol. 125, pp. 465-474, July 2003.
8. Valkov, T. V., and Tan, C. S., "Effect of upstream rotor vortical disturbances on time-averaged performance of axial compressor stators: Part 1 – framework of technical approach and wake-stator blade interactions," *ASME Journal of Turbomachinery*, Vol. 121, pp. 377-386 July, 1999.
9. Valkov, T. V., and Tan, C. S., "Effect of upstream rotor vortical disturbances on time-averaged performance of axial compressor stators: Part 2 – rotor tip vortex/streamwise vortex-stator blade interactions," *ASME Journal of Turbomachinery*, Vol. 121, pp. 387-397 July, 1999.
10. Hutton, T., Leger, T., Johnston, D., and Wolff, M., "High spatial resolution upstream forced response in a transonic compressor," *Journal of Propulsion and power*, Vol. 20, No.4, pp.751-754, July-August 2004.
11. Gorrell, S., Okiishi, T., and Copenhaver, W., "Stator-rotor interactions in a transonic compressor – Part 2 description of a loss-producing mechanism," *ASME Journal of Turbomachinery*, Vol. 125, pp. 336-344, April 2003.